Strongly coupled copper plasma generated by underwater electrical wire explosion

A. Grinenko, V. Tz. Gurovich, A. Saypin, S. Efimov, and Ya. E. Krasik
Physics Department, Technion, 32000 Haifa, Israel

V. I. Oreshkin
Institute of High Current Electronics, SB RAN, 634055 Tomsk, Russia
(Received 31 May 2005; revised manuscript received 28 September 2005; published 5 December 2005)

A number of theoretical approaches to the analysis of the parameters of a discharge channel consisting of strongly coupled plasma generated in the process of underwater electrical wire explosion are presented. The analysis is based on experimental results obtained from discharges employing Cu wire. The obtained experimental data included electrical measurements and optical observations from which information about the dynamics of the water flow was extrapolated. Numerical calculation based on a 1D magnetohydrodynamic model was used to simulate the process of underwater wire explosion. A wide range conductivity model was applied in this calculation and good agreement with a set of experimental data was obtained. A method of determining the average temperature of the discharge channel based on this model and experimental results is proposed, and the limits of this method's applicability are discussed.

DOI: 10.1103/PhysRevE.72.066401 PACS number(s): 52.27.Gr, 52.77.Fv, 52.80.Qj, 52.50.Lp

I. INTRODUCTION

A number of recent studies [1–4] have been devoted to nonideal plasmas which are characterized by the coupling parameter $\Gamma = Z^2 e^2 / akT$, where $a = (3/4\pi n_i)^{1/3}$ is the average distance between the plasma particles and n_i is the plasma density. The parameter Γ characterizes the ratio between the Coulomb and kinetic energies of the plasma particles and, in the case of nonideal, strongly coupled plasmas, $\Gamma \geqslant 1$. The interest in these plasmas is related to sophisticated phenomena associated with their formation and to important applications such as thermonuclear fusion, solid state and plasma-chemical physics, rocket engines, etc. The existence of intermediate states between solid, liquid, gas, and plasma states leads to the appearance of new aggregate states. The main purpose of the experimental studies was to determine the properties of these plasmas and their transport parameters [1–4]. New advanced theoretical models [5–7] have been proposed based on these data.

Electrical wire explosions along with capillary discharges [2,4], *Z*-pinch [8] and other plasmas produced by pulsed power have been widely used to generate nonideal plasmas in a wide range of plasma density and temperature. Underwater electrical wire explosion (UEWE), applied by DeSilva *et al.* [2] for the formation of nonideal plasma, provides better containment of the plasma discharge channel (DC) and generation of high pressures during the discharge. Furthermore, UEWE allows easier optical observations in the visible spectral range, and suppression of some of the instabilities that otherwise develop in nonconfined vacuum or gaseous discharges. However, the assumptions made in experimental data analysis [2] raise a number of problems. Namely, the density and temperature distribution in the cross section of the exploding wire were assumed to be uniform, which implies that the conductivity and current density distributions are also cross-sectionally uniform. Moreover, the pinch effect [8] due to the self-magnetic field of the current, and filamentation instability [9,10] were neglected. In addition channel temperature was not measured directly but was calculated basing on LANL SESAME [11] equation of state (EOS) to relate the measured input energy to the column to the change in temperature and pressure. Next in [2] it was assumed that for a single time step the uniform plasma column undergoes an isochoric addition of electrically input energy, followed by an adiabatic expansion to the new density. This process of temperature calculation is not justified since it ignores nonuniformities of the channel which arise due to compression waves inside the channel and due to magnetic pressure.

In this paper two approaches to the analysis of DC plasma generated during UEWE are presented. The first approach considers a straightforward one-dimensional (1D) magnetohydrodynamics (MHD) calculation. The main difficulty in this calculation was to obtain the correct transport parameters of DC for a large range of density and temperature values that vary with both space and time. An approach to the calculation of conductivity proposed in [12] (reference from the Russian literature) was applied for this purpose. The resulting current and voltage waveforms and DC radius are compared with experimentally obtained data. In the second approach the calculated conductivity tables are used to estimate the average DC temperature. It is shown that this approach yields good results only at the time of the metal-dielectric phase transition which occurs at critical density, where conductivity is virtually independent of the temperature and therefore uniform spatial distribution of temperature in the DC can be assumed.

The paper is divided into four parts. In the first part, experimental results are briefly discussed. In the second part, MHD calculation is presented and transport parameters used in it are established. The third part is devoted to the method of DC temperature estimation based on the calculated conductivity tables and experimental results. The last part of the paper deals with some spectroscopic data.

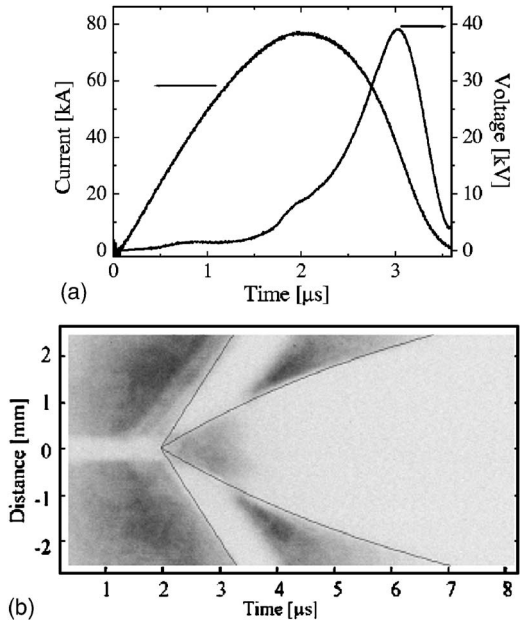

FIG. 1. (a) Typical waveforms of the discharge current and the resistive voltage drop on the exploding Cu wire. (b) Streak shadow image of the exploding Cu wire and the compression waves. The thin black lines describe the contour of the DC boundary used in the computer calculation and the SW front obtained in this calculation, which coincides with the measured one.

II. EXPERIMENTAL RESULTS

The experimental setup used in these experiments is described in detail in [13]. Experiments were carried out using a current generator (5.4 μF, 30 kV, 2.4 kJ). Aperiodical discharge was obtained with Cu wire 85 mm in length and 0.5 mm in diameter. The wire was placed between two electrodes inside a chamber having windows for optical observation and filled with technical water.

A Pierson current transformer and two Tektronix voltage dividers were used to measure the discharge current and voltage drop on the exploding wire, respectively. The inductive voltage $L_w dI/dt + I dL_w/dt$, where L_w is the wire inductance and I is the total current, has been subtracted from the measured value of the voltage drop to obtain the resistive component of the voltage drop along the exploding wire. A shadow image of the wire explosion and generated shock waves (SW) was recorded by a streak EOK-XX camera.

Typical waveforms of the discharge current and the resistive voltage drop on the 500 μm diameter and 85 mm length Cu wire are presented in Fig. 1. A typical shadow streak image of the DC with the resulting SW is presented in Fig. 1(b). Three different waves can be discerned on this image (Fig. 1). The first two waves move with a velocity close to that of sound in water, $c \approx 1.5 \times 10^5$ cm/sec. The generation of these two waves may be attributed to the excess pressure appearing as a result of solid-liquid and liquid-gas phase transitions of the Cu wire. The third wave with a velocity of $1.2c$ appears with the onset of the wire explosion. This wave catches up with and engulfs the preceding waves.

One can see also that during the wire explosion the DC expands at a velocity which varies with time. The obtained

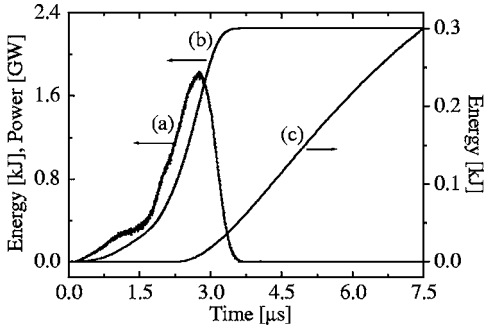

FIG. 2. Time dependencies of (a) electrical input power, (b) absorbed electrical energy, and (c) total energy of the compressed fluid.

evolution of the DC boundary has been used in the hydrodynamic calculation to simulate the generated water flow. The results of the hydrodynamic simulation described in [13] were compared to the data related to the SW trace obtained from the shadow photography [see Fig. 1(b)]. The total measured electrical input power, energy and calculated energy of the water flow are shown in Fig. 2.

III. MAGNETOHYDRODYNAMIC MODEL

A one dimensional, single temperature approximation of UEWE is considered. In the case of cylindrical geometry, MHD equations in Lagrange formulation have the following form [14,15]:

$$\frac{\partial \rho}{\partial t} + \frac{1}{r}\frac{\partial (r\rho v)}{\partial r} = 0, \tag{3.1}$$

$$\rho \frac{\partial v}{\partial t} + \rho v \frac{\partial v}{\partial r} = -\frac{\partial p}{\partial r} - \frac{1}{c} j_z B_\varphi, \tag{3.2}$$

$$\rho \frac{\partial \varepsilon}{\partial t} + \rho v \frac{\partial \varepsilon}{\partial r} = -p \frac{1}{r}\frac{\partial (rv)}{\partial r} + \frac{j_z^2}{\sigma} + \frac{1}{r}\frac{\partial}{\partial r}\left(r\kappa \frac{\partial T}{\partial r} \right), \tag{3.3}$$

$$\frac{1}{c}\frac{\partial B_\varphi}{\partial t} = \frac{\partial E_z}{\partial r}, \quad j_z = \frac{c}{4\pi r}\frac{\partial (rB_\varphi)}{\partial r}, \tag{3.4}$$

$$j_z = \sigma E_z, \tag{3.5}$$

$$P = P(\varepsilon, \rho), \quad T = T(\varepsilon, \rho), \tag{3.6}$$

$$\sigma = \sigma(\varepsilon, \rho), \quad \kappa = \kappa(\varepsilon, \rho), \tag{3.7}$$

where ρ and T are the density and temperature of the material; p and ε are the pressure and energy density of the material; σ and κ are the coefficients of electrical and heat conductivities; v is the radial component of the velocity; E_z is the longitudinal component of the electric field; j_z is the longitudinal component of electric current density; B_φ is the azimuthal component of the magnetic field. System (3.1)–(3.7) was solved numerically using MHD code in Lagrange mass coordinates. Here explicit scheme "cross" has

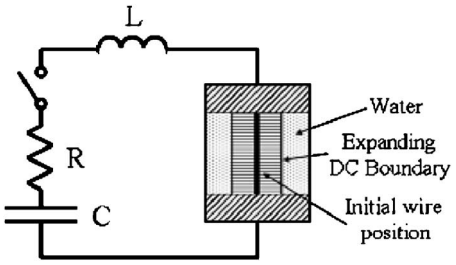

FIG. 3. Sketch of wire explosion geometry and electric circuit. $C=5.4$ μF, $L=320$ nH, and $R=0.1$ Ω.

been used to resolve hydrodynamic equations (3.1)–(3.3) [14]. For the solution of Maxwell equations (3.4) together with Ohm law (3.5) and also for the solution of heat conductivity, an implicit "flow chaser" method was used [14]. The calculation grid consisted of two areas, namely DC material and the water (see Fig. 3). It was assumed that during the discharge water conductivity is negligibly small, so that all the current flows through the wire material and the water exerts only a hydrodynamic effect. This assumption seems to be correct in the case of aperiodical discharge.

The boundary condition used for Maxwell equations was

$$B_{\varphi}(R) = \frac{2I_w}{cR}, \tag{3.8}$$

where R is the DC channel radius and I_w is the current flowing through the DC. The value of the DC current was determined from the simultaneous solution of Maxwell and electrical circuit (Fig. 3) equations.

The system of MHD equations is completed with EOS [Eq. (3.6)] and related transport parameters [Eq. (3.7)]. EOS of copper was obtained from More's theoretical model [16]. More's quotidian equation of state (QEOS) is a general purpose EOS model in which electronic properties are obtained from a modified Thomas-Fermi statistical model, while ion thermal motion is described by a multiphase EOS combining Debye, Grüneisen, Lindemann, and fluid scaling laws. EOS of water was taken from the compiled experimental data of Bridgman [17]. Electrical conductivity of the DC material was evaluated by the semiempirical method described in [12]. The only fitting parameter in this model is the value of conductivity at critical point σ_{cr} which was found by comparing a large set of experimental results with the MHD calculation. The conductivity found using this approach is strongly dependent on the state of the matter. Basically, in the metallic part of the phase space the conductivity decreases with rising temperature, whereas in the plasma part of the phase space the conductivity increases. The decrease in metallic conductivity caused by input electric energy and the resultant Ohmic heating is the process that finally causes the current to be rapidly interrupted and the metallic wire to explode. The corresponding values of heat transfer coefficients are found from the Wiedemann-Franz law [18].

The values of extrapolated critical density, temperature, pressure, and conductivity for copper are $\rho_{cr}=3.82$ g/cm^3, $T_{cr}=0.96$ eV, $p_{cr}=109\times10^8$ Pa, and $\sigma_{cr}=7.19\times10^5$ S/m, respectively. The corresponding plot of the electrical conductivity of copper calculated according to the Bakulin-Kuropatenko-Luchinskii (BKL) model [12] for temperatures ranging from 0.02 eV to 6 eV is shown in Fig. 4. In addition, the values of the conductivity calculated according to the BKL model for two temperatures (10000 K and 30000 K) are shown in Fig. 5 (in solid diamonds line) for comparison with conductivity values calculated according to other models and with experimental results [2]. One can see that the conductivity values calculated according to the BKL model are in good correspondence with the experimental results [2] for higher temperatures, e.g., 3 eV [Fig. 5(b)], but

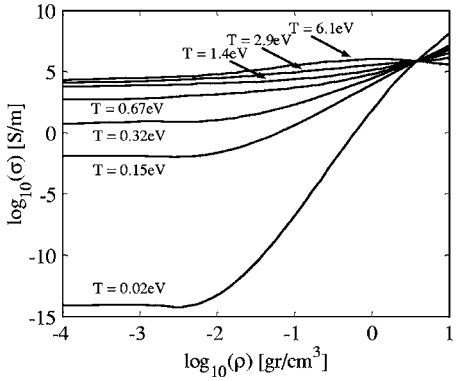

FIG. 4. Conductivity values of copper calculated for temperature values ranging from 0.01 eV to 6 eV using the Bakulin-Kuropatenko-Luchinskii [12] model.

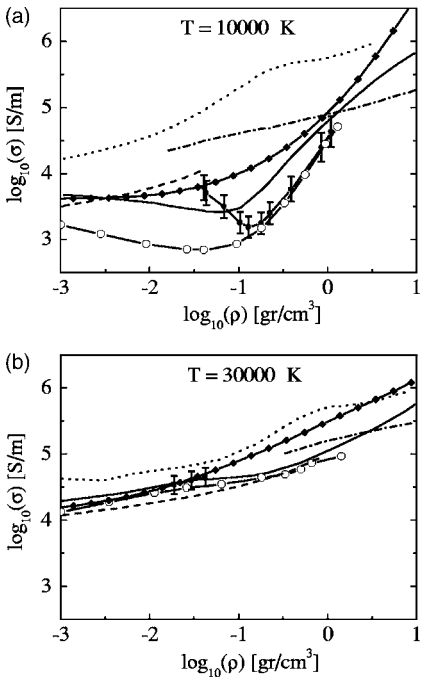

FIG. 5. Electrical conductivity of copper plasma at two temperatures. Theoretical models are from Ebeling *et al.* [19], solid line, Lee and More [20], dotted line, Ichimaru and Tanaka [21], dashed line, Kurilenkov and Valuev [22], dash-dotted line, Redmer [7], solid circles markers line. Theoretical model of Bakulin-Kuropatenko-Luchinskii [12] used in our calculation is shown by the solid line with diamond markers and experimental data from [2] is shown by squares with 5% error bars.

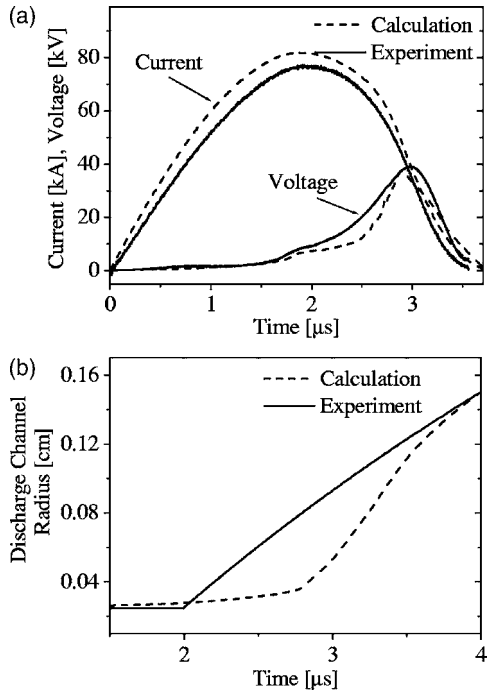

FIG. 6. (a) Current and voltage waveforms obtained from the aperiodic discharge using 85 mm length 510 μm diameter Cu wire and 5.4 μF, 30 kV charged capacitors. (b) Trajectory of moving interface of the DC and water. Experimental data are shown by the solid line; numerical MHD calculation are shown by the dashed lines.

have a worse agreement for lower temperatures, e.g., 1 eV [Fig. 5(a)]. However, in this range the BKL model data complies with other theoretical models.

Comparison of experimentally measured current and voltage waveforms and the channel radius obtained with MHD model calculation results allows the conformity of EOS and conductivity models used in calculations to be assessed. In Fig. 6(a) current and voltage waveforms measured and numerically calculated using the MHD model are shown for the explosion of 85 mm length, 510 μm diameter Cu wire when 30 kV charged 5.4 μF capacitors were applied to the wire. Total inductance of the circuit is 320 nH and circuit resistance, including resistance of capacitors, current holders and switches, is 0.1 Ω. One can see a good correspondence between the calculated and experimental results. Amplitudes of the voltage and current as well as characteristic features such as instants of phase transitions coincide. However, some discrepancy can be observed in the measured and calculated DC radius [see Fig. 6(b)]. The experimental curve of DC radius is extrapolated from the shadow image of the DC when it separates from the SW. Before the separation, the DC border is assumed to be the border of the light emitting zone. In this manner the solid curve in Fig. 6(b) is obtained. However, one can see that the solid line differs from the calculated evolution of the DC radius which is shown as a dashed curve.

The calculated and the measured radii become almost the same when the separation of DC and SW start to be observable, namely after 3.7 μs with respect to the beginning of the discharge current. It is reasonable to assume that the interpolation of the DC radius at the initial stage of the discharge, i.e., during the light emitting stage, as the size of the light emitting zone is not entirely correct. Though the light emitting zone is associated with the expanding DC, a poor spatial resolution ($\leqslant$200 μm) during the period of light emission does not allow us to extrapolate the DC boundary more accurately than shown in Fig. 6(b). One can see that according to this extrapolation, the DC boundary starts expanding with nonzero initial velocity, whereas this velocity should increase gradually from zero. Note that according to the MHD simulation, the expansion of the DC starts from zero velocity, which is more reasonable. The indicated discrepancy between MHD and the DC boundary extrapolated from experimental streak image can lead to overestimation of the DC temperature and also underestimation of the DC pressure at its boundary.

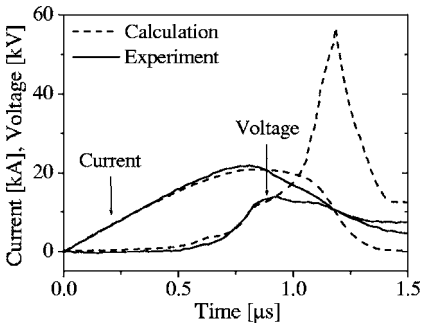

FIG. 7. Experimental—dashed and numerical—solid current and voltage waveforms of 45 mm length 200 μm diameter Cu wire explosion using 15 kV, 5.4 μF capacitors.

One can see from Fig. 1(b) that the SW is generated in the vicinity of the DC at $\sim$2 μs from the beginning of the discharge current, and one therefore may be led to suppose that this moment corresponds to the onset of the DC expansion. However, it was shown in Sec. II that pressure waves in water are generated prior (at $\sim$1.5 μs from the discharge current beginning) to the onset of the DC expansion and the reasons for this were discussed in Sec. II. Similarly, the appearance of the SW at $\sim$2 μs [see Fig. 1(b)] may be unrelated to the expansion of the DC but rather attributable to the drop in the magnetic pressure. Indeed, at $\sim$2 μs, the discharge current reaches its maximal value and begins to fall. Therefore, from this moment the compensation of the hydrodynamic pressure by the magnetic pressure weakens. The appearance of this pressure difference at the boundary of the DC may cause the generation of the SW.

The situation is somewhat different in the case of quasiperiodic discharge when the energy stored in capacitors is larger than the sublimation energy of wire material. In this case, after the wire material evaporates and loses its metallic conductivity, a secondary electrical discharge occurs restoring the high conductivity of the DC. The latter limits the active voltage drop and the energy density which can be deposited in the DC. This case is depicted in Fig. 7 where the explosion of 45 mm length, 200 μm diameter Cu wire supplied by 5.4 μF capacitors charged to 15 kV is shown. One can see that until the time τ_d of wire evaporation, which occurs at $\tau_d \sim 0.9$ μs with respect to the beginning of the

discharge current, the measured and calculated current and voltage are in good correspondence. However, after the evaporation, the experimentally measured voltage stops growing, whereas the calculated voltage continues increasing to values almost five times higher than in the experiment. The results shown indicate that, in order to obtain agreement with experiment, a model which includes dynamic breakdown phenomena is essential.

In summary, the described UEWE's are subcritical, i.e., the wire expansion starts before critical pressure and critical temperature are achieved. The maximal value of the temperature inside the DC calculated for 85 mm length, 510 μm diameter, 30 kV Cu wire explosion was $\sim$1 eV.

IV. ANALYSIS OF EXPERIMENTAL RESULTS BASED ON UNIFORM SPATIAL DISTRIBUTION ASSUMPTION

The task of defining plasma parameters in the process of UEWE is rather complicated for a number of reasons the most important of which are the small radial dimensions of the DC plasma and its opacity. In addition, high density and nonideality of the DC plasma limit the use of standard spectroscopic techniques and make analysis of experimental data very complicated. Therefore experimental measurements of DC temperature are usually limited to the measurement of the surface temperatures [2], and temperature, pressure, and density distribution are assumed to be spatially uniform. The assumption of uniform pressure distribution is valid only after the current stops flowing through the DC, since otherwise the pressure of the self-magnetic field of the DC current and compression waves traveling inside the channel must bring in nonuniform hydrodynamic pressure distribution.

In this part of the paper we present an approach for obtaining average DC plasma parameters based on the use of EOS tables [16] and calculated conductivity tables [12] that have been used in MHD calculation described in previous section. In this approach spatially homogeneous distribution of DC parameters is assumed, and the plasma parameters are extrapolated from the obtained experimental current and voltage waveforms and optical observations. Thus, assuming uniform temperature and density distribution, which leads to uniform conductivity distribution, since $\sigma(r)=\sigma(\rho(r),T(r))$, the temperature is found from the solution of the equation

$$\sigma\left(\rho_0\left(\frac{R_0}{R}\right)^2,T\right)=\frac{L}{\pi R^2}\frac{I}{V}, \tag{4.1}$$

where R_0 is the initial radius of the wire, R is the DC radius at time t, L is the length of the discharge gap, ρ_0 is the initial density of the wire material, and I and V are the current and voltage at time t, respectively. The temperature is obtained from Eq. (4.1) by finding the value of T according to the calculated conductivity table for which Eq. (4.1) is satisfied. Resulting temperatures are shown in Fig. 8. On the same plot corresponding average temperatures calculated using the results of numeric computation (see Sec. III) as

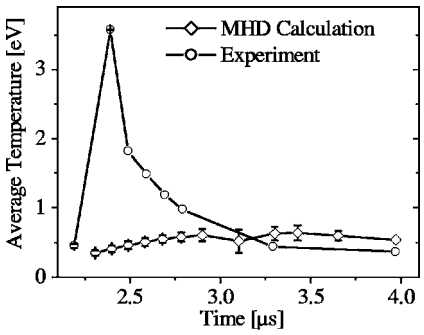

FIG. 8. Average DC temperature obtained from the MHD calculation (diamonds) and the average DC temperature obtained from the average conductivity method (circles).

$$\langle T\rangle=\int_0^R \rho r T\,dr \Big/ \int_0^R \rho r\,dr \tag{4.2}$$

are shown. One can see that the temperature found from the experimental data by the described method is much larger than the calculated average temperature. As has been pointed out, the reason may be found in the incorrect estimation of the DC radius at the initial stage of the discharge before the SW separates from the DC. After the separation at $\tau_d \approx 3.5$ μs the temperature values obtained by both methods agree satisfactorily within the 30% limit.

In Fig. 9 the plot of the pressure at the DC-water interface boundary is shown. Here the values of boundary pressure obtained from MHD calculation and the values of the pressure deduced from the streak photograph, using the hydrodynamics of the water, as in [13] are compared. Also here, one can see that the pressure values received from the MHD calculation exceed the experimental values. This discrepancy has an obvious reason since the DC boundary velocity predicted by MHD calculation is higher than the velocity estimated from experimental observation [Fig. 6(b)]. After the DC boundary and the SW separate from each other at $\tau_d \approx 3.5$ μs, the calculated and observed DC boundary trajectories join together and corresponding calculated and experimentally obtained DC boundary pressures take the same value.

The results described indicate that the DC temperature can be estimated with the assumption of uniform spatial distribution within a 30% error only in the relatively late stages

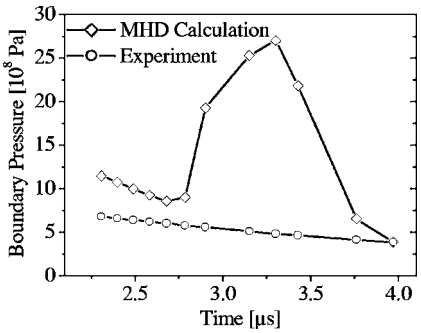

FIG. 9. Pressure at the DC-water interface obtained from MHD calculation (diamonds), and from the experimental-theoretical method described in [13] (circles).

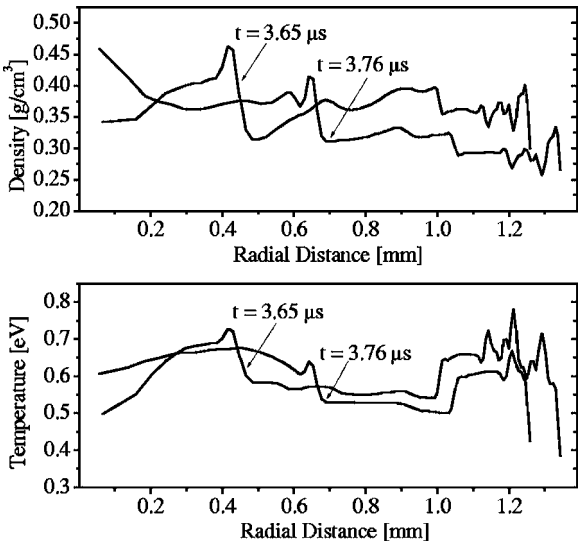

FIG. 10. Numerically calculated pressure and temperature profiles inside the DC after the onset of separation of DC and shock wave generated in water.

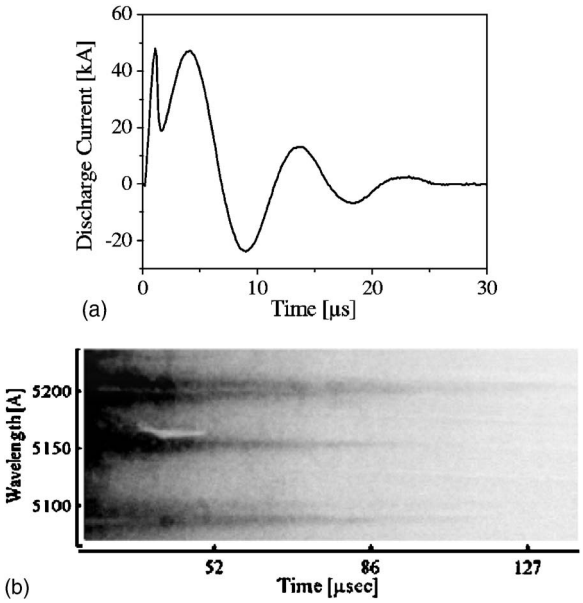

FIG. 11. (a) Current waveform of 45 mm length 200 μm diameter explosion of Cu wire using 15 kV, 5.4 μF capacitors. (b) Streak image of emitted Cu I lines.

of the discharge, when the DC boundary can be observed separately from the SW. The same conclusion concerns the estimated pressure of the DC boundary. The 30% error in temperature estimation could be the result of actual spatial nonuniformity of DC channel parameters and various dynamical effects, as demonstrated in Fig. 10, where temperature and density profiles inside the DC channel at two different time instants of the discharge, 3.65 μs 3.76 μs, are shown. Two SW traveling inside the DC can be seen. One SW is reflected from the boundary and moves towards the center and the other SW is reflected from the center and propagates outwards. These spatial nonuniformities of both the temperature and the density, which determine the value of local conductivity, can lead to the difference between the average calculated temperature and the temperature estimated from experimental data when spatial uniformity is assumed.

V. SPECTROSCOPIC ANALYSIS

Experimental evidence of the existence of high temperature and density gradient during wire explosion has been obtained in spectroscopic measurements. In Fig. 11(a) current and voltage waveforms of the quasiperiodic discharge regime achieved with 15 kV explosion of 200 μm diameter 45 mm length Cu wire are shown. In Fig. 11(b) the corresponding streak image of emitted Cu I lines is shown. The vertical axis of Fig. 11(b) is the wavelength axis, and the horizontal axis denotes time. The first notable feature of this spectrum is that the measured light emission continues for $\sim$100 μs after the end of the discharge current. The other feature is that one initially obtains absorption lines observable on the background of substantially broadened Cu I lines. Within $\sim$120 μs after the end of the discharge current, the spectrum changes to the Cu I emission spectrum. The modeling of the Stark profile of the Cu I[$4p(2P)$-$4d(2D)$] spectral line which neglects opacity allows the electron density to be estimated; immediately after the DC current ends it was found to be $\sim 10^{18}$ cm^{-3}.

The relatively thin absorption lines observed on the background of broadened emission spectrum suggest that there is an inner region with dense hot material. This hot region emits light which passes through a spatial region of colder matter. The latter absorbs the emitted light. Indeed, such a density profile may arise since 20 μs after the beginning of the discharge current, the Cu wire material has passed the critical point and is in a state when the conductivity grows with the temperature. The latter may give rise to filamentation instability [9,10] resulting in a hot core.

VI. CONCLUSION

A number of theoretical approaches to the analysis of the strongly coupled plasma parameters generated by UEWE are presented. Good agreement between numeric MHD calculation and experimental results was obtained. A wide range, semiempirical, conductivity model [12] was tested and successfully applied in numerical calculations. This conductivity was used to determine the temperature of the DC using experimental data, which included electrical measurements and optical observations, and assumed that the spatial distribution of DC plasma parameters is uniform. It was shown that this method is applicable only at relatively late times of the discharge, when the separation of DC and shock wave generated in surrounding water occurred. At that time the error in estimated temperature can be ascribed to the nonuniformity of the DC which is demonstrated by numerical calculation.

Some experimental evidence giving clues of such nonuniform density and temperature distribution was obtained by spectroscopic measurements.

ACKNOWLEDGMENTS

We wish to thank Andreas Kemp for generously providing the MPQ^{EOS} code for the calculation of the equation of state based on the QEOS model [16] and Evgenii Stambulchik for providing Stark broadening analysis. This research was supported by the Israel Science Foundation Grant No. 1210/04. The work of V.I.O. was supported by the RFBR Grant No. 05-02-16845.

[1] W. DeSilva and H. J. Kunze, Phys. Rev. E **49**, 4448 (1994).
[2] W. DeSilva and J. D. Katsourus, Phys. Rev. E **57**, 5945 (1997).
[3] A. Kloss, T. Motzke, R. Grassjohan, and H. Hess, Phys. Rev. E **54**, 5851 (1996).
[4] J. F. Benage, Jr., W. R. Shanahan, E. G. Sherwood, L. A. Jones, and R. J. Trainor, Phys. Rev. E **49**, 4391 (1994).
[5] M. P. Desjarlais, J. D. Kress, and L. A. Collins, Phys. Rev. E **66**, 025401 (2002).
[6] M. P. Desjarlais, Contrib. Plasma Phys. **41**, 267 (2001).
[7] R. Redmer, Phys. Rev. E **59**, 1073 (1999).
[8] T. J. Nash *et al.*, Phys. Plasmas **11**, L65 (2004).
[9] R. J. Goldston and P. H. Rutherford, *Introduction to Plasma Physics* (IOP, Bristol, 1995).
[10] V. E. Fortov and I. T. Iakubov, *The Physics of Non-Ideal Plasma* (World Scientific, Singapore, 2000).
[11] SESAME: The Los Alamos National Laboratory Equation of State Database, Report No. LA-UR-92-3407, edited by S. P. Lyon and J. D. Johnson, Group T-1 (unpublished).
[12] Yu. D. Bakulin, V. F. Kuropatenko, and A. V. Luchinskii, Sov. Phys. Tech. Phys. **21**, 1144 (1976).
[13] A. Grinenko, A. Sayapin, V. Tz. Gurovich, S. Efimov, J. Felsteiner, and Ya. E. Krasik, J. Appl. Phys. **97**, 023303 (2005).
[14] I. V. Oreshkin, V. S. Sedoi, and L. I. Chemezova, Appl. Phys.0947-8396 (in Russian) **3**, 94 (2001).
[15] I. V. Oreshkin, R. B. Baksht, A. Yu. Labezkii, A. G. Rousskikh, A. V. Shishlov, P. R. Levashov, K. V. Khishchenko, and I. V. Glazyrin, Tech. Phys. **49**, 843 (2004).
[16] R. M. More, K. H. Warren, D. A. Young, and G. B. Zimmerman, Phys. Fluids **31**, 843 (1988).
[17] F. A. Baum *et al.*, *Physics of Explosion* (Nauka, Moscow, 1975) (in Russian).
[18] G. Wiedemann and R. Franz, Ann. Phys. **89**, 497 (1853).
[19] W. Ebeling, A. Förster, V. Fortov, V. Gryaznov, and A. Polishchuk, *Thermophysical Properties of Hot Dense Plasmas*, Teubner-Texte zur Physik Vol. 25 (Teubner Verlagsgesellschaft, Stuttgart, 1991), pp. 274–275.
[20] Y. T. Lee and R. M. More, Phys. Fluids **27**, 1273 (1984).
[21] S. Ichimaru and S. Tanaka, Phys. Rev. A **32**, 1790 (1985).
[22] K. Kurilenkov and A. A. Valuev, Beitr. Plasmaphys. **24**, 161 (1984).